Geoscience Frontiers 14 (2023) 101516

HOSTED BY

Contents lists available at ScienceDirect

Geoscience Frontiers

journal homepage: www.elsevier.com/locate/gsf

Research Paper

Carbonaceous aerosol transport from the Indo-Gangetic Plain to the Himalayas: Carbon isotope evidence and light absorption characteristics

Pengfei Chen [a], Shichang Kang [a,b,*], Chaoliu Li [a,b], Zhaofu Hu [a], Lekhendra Tripathee [a], Mukesh Rai [a], Tao Pu [a], Xiufeng Yin [a], Örjan Gustafsson [c,d]

[a] State Key Laboratory of Cryospheric Science, Northwest Institute of Eco-Environment and Resources, Chinese Academy of Sciences (CAS), Lanzhou 730000, China
[b] University of Chinese Academy of Sciences, Beijing 100049, China
[c] Department of Environmental Science, The Bolin Centre for Climate Research, Stockholm University, Stockholm 10691, Sweden
[d] The Bolin Centre for Climate Research, Stockholm University, Stockholm 10691, Sweden

ARTICLE INFO

Article history:
Received 27 June 2022
Revised 22 October 2022
Accepted 23 November 2022
Available online 29 November 2022
Handling Editor: E. Shaji

Keywords:
Carbonaceous aerosol
Long-range transport
Carbon isotope
Source apportionment
Light absorption
The Himalayas

ABSTRACT

The Indo-Gangetic Plain (IGP) is a major regional and global emitter of atmospheric pollutants, which adversely affect surrounding areas such as the Himalayas. We present a comprehensive dataset on carbonaceous aerosol (CA) composition, radiocarbon ($\Delta^{14}C$) -based source apportionment, and light absorption of total suspended particle (TSP) samples collected over a 3-year period from high-altitude Jomsom in the central Himalayas. The 3-year mean TSP, organic carbon (OC), and elemental carbon (EC) concentrations were 92.0 ± 28.6, 9.74 ± 6.31, and 2.02 ± 1.35 μg m^{-3}, respectively, with the highest concentrations observed during the pre-monsoon season, followed by the post-monsoon, winter, and monsoon seasons. The $\Delta^{14}C$ analysis revealed that the contribution of fossil fuel combustion (f_{fossil}) to EC was 47.9% ± 11.5%, which is consistent with observations in urban and remote regions in South Asia and attests that EC likely arrives in Jomsom from upwind IGP sources via long-range transport. In addition, the lowest f_{fossil} (38.7% ± 13.3%) was observed in winter, indicating large contributions in this season from local biomass burning. The mass absorption cross-section of EC (MAC_{EC}: 8.27 ± 1.76 m^2/g) and water-soluble organic carbon (MAC_{WSOC}: 0.98 ± 0.45 m^2/g) were slightly higher and lower than those reported in urban regions, respectively, indicating that CA undergo an aging process. Organic aerosol coating during transport and variation of biomass burning probably led to the seasonal variation in MAC of two components. Overall, WSOC contributed considerably to the light absorption (11.1% ± 4.23%) of EC. The findings suggest that to protect glaciers of the Himalayas from pollution-related melting, it is essential to mitigate emissions from the IGP.

© 2022 China University of Geosciences (Beijing) and Peking University. Published by Elsevier B.V. on behalf of China University of Geosciences (Beijing). This is an open access article under the CC BY-NC-ND license (http://creativecommons.org/licenses/by-nc-nd/4.0/).

1. Introduction

The Himalayas are impacted by Atmospheric Brown Clouds (ABC), with large forcing from black carbon (BC or elemental carbon: EC) in snow cover and glacier estimated to occur in this region (Ramanathan et al., 2007; Ramanathan and Carmichael, 2008; Flanner et al., 2009; Yang et al., 2018; Kang et al., 2020, 2022). The seasonally prevalent ABC is rich in carbonaceous aerosols (CA), which often originates in the Indo-Gangetic Plain (IGP) and extends downwind over the Himalayan range. Sometimes it even reaches heights of more than 3 km asl through convection and advection (Hindman and Upadhyay, 2002; Bonasoni et al., 2008; Marinoni et al., 2010; Cong et al., 2015; Lüthi et al., 2015; Li et al., 2016a; Rai et al., 2022). CA is composed of organic carbon (OC) and EC. It affects the regional climate through absorbing and scattering of solar radiation and alters hydrological cycles and storm frequencies (Menon et al., 2002; Meehl et al., 2008; Bond et al., 2013; Ji et al., 2015). Particularly, it is accelerating the Himalayan glacier melting through atmospheric heating and albedo reduction (Hansen and Nazarenko, 2004; Xu et al., 2009; Zhang et al., 2017; Kang et al., 2019, 2022).

Light absorption characteristics such as the mass absorption cross-section (MAC) of EC and brown carbon (BrC, light-absorbing component of OC) are essential in elucidating our understanding of the effects of CA on the climate and cryosphere loss (Sun et al., 2007; Alexander et al., 2008; Bahadur et al., 2012;

* Corresponding author at: State Key Laboratory of Cryospheric Science, Northwest Institute of Eco-Environment and Resources, Chinese Academy of Sciences (CAS), Dong Gang Xi Road, Chengguan District, Lanzhou 730000, PR China.
E-mail address: shichang.kang@lzb.ac.cn (S. Kang).

https://doi.org/10.1016/j.gsf.2022.101516
1674-9871/© 2022 China University of Geosciences (Beijing) and Peking University. Published by Elsevier B.V. on behalf of China University of Geosciences (Beijing). This is an open access article under the CC BY-NC-ND license (http://creativecommons.org/licenses/by-nc-nd/4.0/).

Chung et al., 2012; Hodnebrog et al., 2014). However, in situ data are still rare at the Himalayas. In addition, data sets focusing on the source apportionment of CA in this region are sparse (Li et al., 2016a), limiting our ability to implement an effective mitigation strategy to counteract climatic effects and health hazards from the air pollution.

The radiocarbon ($\Delta^{14}C$) isotope fingerprint of EC is a powerful diagnostic tool for distinguishing and quantifying the contributions of fossil fuel and biomass combustion (Szidat et al., 2004; Gustafsson et al., 2009; Zhang et al., 2014, 2015; Li et al., 2016a; Fang et al., 2018; Bikkina et al., 2019). Several studies have quantified the fossil contribution to EC (50% ± 8%) and provided clear distribution data for South Asia (Gustafsson et al., 2009; Budhavant et al., 2015; Winiger et al., 2017; Dasari et al., 2020). Li et al. (2016a) identified consistent source contributions from fossil fuels (46% ± 11%) over the central Himalayas within the IGP, and the biomass burning contribution was found to increase from south to north along two transects. However, only a few samples were chosen to measure $\Delta^{14}C$ in that study.

We therefore present the results of CA based on data last for 3-years (April 2012 to April 2014 and October 2017 to September 2018) in Jomsom, to improve the understanding of the characteristics of CA in the high Himalayas. At the same time, year-round radiocarbon data were investigated to distinguish fossil-derived from biomass-derived EC to provide direct evidence of the CA reaching the Himalayas and the Tibetan Plateau. In addition, the seasonal variations in the MAC of EC and water-soluble organic carbon (WSOC) were investigated to determine their efficiency for absorbing solar radiation. This study broadens our knowledge of the sources of CA sources in this hotspot and expands the understanding of their climate effects.

2. Materials and methods

2.1. Sampling site and total suspended particle collection

Jomsom (28.87° N, 83.73° E, 2900 m asl) is a small village in the Mustang district of Nepal. This site is located in the Kali Gandaki Valley that cuts across the Himalayas at the transition point between South Asia and the Tibetan Plateau (Fig. 1). This area is well-known for its strong mountain valley winds, which enable the advection of pollutants from the lower plains (Dhungel et al., 2018). The study site is pristine, with few households and fields. Many tourists visit this area during the dry season to trek in the Annapurna Circuit. The climate of this area is dominated by the South Asian monsoon circulations and comprises four distinct seasons; winter (December–February), pre-monsoon (March–May), monsoon (June–September), and post-monsoon (October–November). Jomsom has one of the lowest precipitations in Nepal, with <300 mm of annual rainfall (Tripathee et al., 2020).

A total suspended particle (TSP) sampler was placed on the rooftop (3 m above the ground) of a single-story laboratory building, which is at the southern end of a terrace exposed to the strong wind flow of the Kali Gandaki Valley (Fig. 1). The nearest road is at 200 m horizontal distance and 90 m below the station. The village of Syang (population of approximately 100) is located 600 m south from the station at an elevation of 100 m lower. The town of Jomsom (population approximately 2000) lies 1–2 km north. One dilapidated hotel is situated 450 m north at approximately the same elevation.

A total of 173 TSP samples were collected on prebaked quartz fiber filters (90-mm diameter, Whatman plc., Maidstone, UK) by a sampler fitted with a TSP cyclone (flow rate: 100 L min^{-1}, KC-120H: Qingdao Laoshan Applied Technology Institute, Qingdao City, China), with samples collected for 24-h periods every 6 days from April 2012 to April 2014 and from October 2017 to September 2018. Field blank filters were placed in the sampler with no air drawn through them. The pretreatment of the filters is showed in Supplementary Data Text S1.

2.2. CA concentration measurements

A punch aliquot (0.5025 cm^2) of the quartz fiber filter samples was analyzed for OC and EC using a thermal/optical carbon aerosol analyzer (DRI Model 2001A, Desert Research Institute of the University of Nevada, Reno, NV, USA). Thermal chemical analysis to determine OC and EC concentrations was performed using the thermal/optical reflectance method in accordance with the Interagency Monitoring of Protected Visual Environments (IMPROVE) protocol (Supplementary Data Text S1) (Cao et al., 2003; Chow et al., 2007). Concentrations of WSOC were measured using a total OC (TOC) analyzer (5000A, Shimadzu, Kyoto, Japan). The light absorption spectra between 200 and 800 nm of the WSOC were measured to 5-nm precision using an ultraviolet–visible spectrophotometer (SpectraMax M5; Supplementary Data Text S2). The exact treatment method was detailed in our previous studies (Li et al., 2016b; Chen et al., 2020). The CA concentrations were blank corrected by subtracting the mean of the field blanks. The MAC was calculated using the method outlined in previous studies (Supplementary Data Text S3) (Weingartner et al., 2003; Ram and Sarin, 2009; Cheng et al., 2011).

2.3. CO_2 isolation and carbon isotope analysis

The EC fraction was isolated, and the produced CO_2 was collected using modified equipment to identify its radiocarbon signature (e.g., Zencak et al., 2007; Li et al., 2016a; Gustafsson et al., 2009). The present method has been detailed and tested in various ways as reported in methods sections of peer-reviewed scientific publications (Chen et al., 2013; Winiger et al., 2015, 2016, 2019). One of the most common, well-established thermal-optical methods—NIOSH 5040 was used in the present study for consistent comparisons between different sites and time-periods (Birch and Cary, 1996). The procedure is introduced briefly. First, a filter with area that contains 60–120 μg of EC for each sample was acidified using fumigation in open glass petri dishes in a desiccator over 12 M hydrochloric acid for 24 h to remove carbonates and subsequently dried at 60 °C for 1 h. Filter subsamples were placed inside a SUNSET analyzer for oxidation to CO_2. The resultant CO_2 was diverted and purified online through magnesium perchlorate and silver wool traps to remove water and halogen-containing gases, respectively. Subsequently, the purified CO_2 was cryotrapped in liquid N_2 and flame-sealed in glass ampoules. The ampoules were then transferred to the US National Science Foundation's National Ocean Sciences Accelerator Mass Spectrometry facility at the Woods Hole Oceanographic Institution (Woods Hole, MA, USA). The radiocarbon analysis results are reported as per mill deviations ($\Delta^{14}C$) from the National Bureau of Standards oxalic-acid standard. Because of the inert (unreactive) nature of EC, minimal isotopic fractionation during long-range transport was expected.

2.4. Calculation of radiocarbon-based source contributions

The fractional contributions of radiocarbon from fossil fuel sources (f_{fossil}) and of contemporary biomass and biogenic sources were determined using the following isotopic mass balance equation:

$$\Delta^{14}C_{sample} = \Delta^{14}C_{fossil} \cdot f_{fossil} + \Delta^{14}C_{biomass} \cdot (1 - f_{fossil})$$

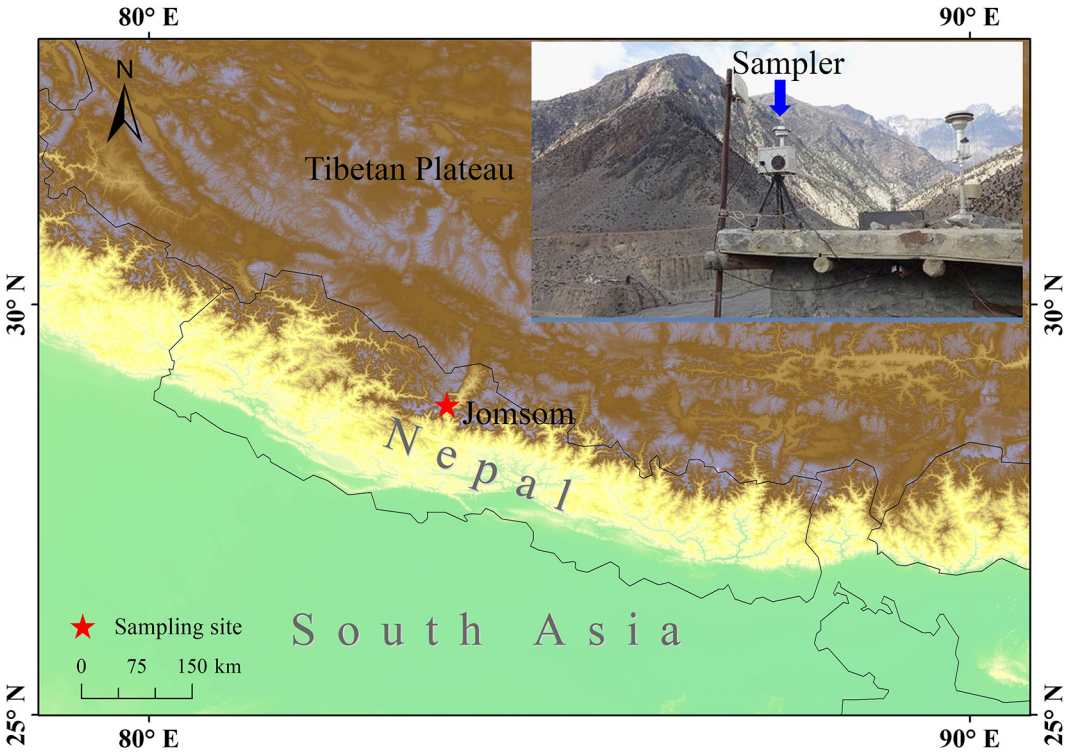

Fig. 1. Overview map showing sampling site and atmospheric observatory in Jomsom.

where $\Delta^{14}C_{sample}$ is the measured radiocarbon concentration of a sample and $\Delta^{14}C_{fossil}$ is −1000‰. The $\Delta^{14}C_{biomass}$ end-member is between +50‰ and +225‰. The first value corresponds to the $\Delta^{14}C$ of contemporary CO_2 and thus to freshly produced biomass (Graven et al., 2012), and the second is the $\Delta^{14}C$ of wood logged in the 1990 s – 2000 s (Klinedinst and Currie, 1999; Zencak et al., 2007). An end member value of +200‰ was used following the study of Li et al. (2016a) which have measured the $\Delta^{14}C$ for two aerosol samples of Jomsom.

During thermal-optical analysis of CA, it is well-recognized that a certain amount of the OC is pyrolyzed, forming pyrogenic carbon (PyrC). The PyrC concentrations of all 12 samples were given in Supplementary Data Table S1. It may be speculated that this PyrC may be transferred into the EC phase, and thereby possibly affecting the isotopic composition of isolated EC. This would lead to an overestimation of the fraction of biomass burning, given that OC is typically of mainly contemporary origin. To test the sensitivity of the obtained ^{14}C-based source apportionment results to a putative exchange in the isolation between method-induced PyrC, a sensitivity analysis, based on instrument-generated PyrC has been performed (Supplementary Data Table S2). According to study conducted at two receptor observatories of South Asia, a putative PyrC to EC transfer of 25% EC was calculated from this isotopic mass balance criterion (Budhavant et al., 2015). From this estimate, we concluded that even if the PC contribution to EC was as high as 25%, this would lead to a maximum shift in relative fossil fuel contribution of 8%, which does not significantly change the final conclusions found in this study (Supplementary Data Table S2).

2.5. Backward air-mass trajectories and fire spots

A 5-day backward-trajectory analysis was conducted using the Hybrid Single-Particle Lagrangian Integrated Trajectory (HYSPILT4) model at a height of 500 m above the measurement site and the Global Data Assimilation System to reveal the transport pathways of the air mass that reached Jomsom (Draxler and Rolph, 2012). This height is suitable for considerations of both the long-range transport and transport in the planetary boundary layer. Additionally, active fire spots (region: 15°-45° N, 60°-100° E) over four seasons from October 2017 to September 2018 were identified using the Fire Information for Resource Management System (https://earthdata.nasa.gov/earth-observation-data/near-real-time/firms/). Furthermore, TrajStat software was employed to identify clusters and determine concentration weighted trajectories (CWTs) (Wang et al., 2009).

3. Results and discussion

3.1. Concentration of CA and temporal variations

The pollutant concentrations during the sampling period are listed in Table 1. The mean TSP concentration was 92.0 ± 28.6 μg m^{-3} (range, 40.8–199.5 μg m^{-3}) for the entire sampling period. The mean OC and EC concentrations were 9.74 ± 6.31 and 2.02 ± 1.35 μg m^{-3}, respectively. On average, OC and EC accounted for 10.58% and 2.20% of the TSP. The mass concentration of WSOC varied from 0.70 to 23.5 μg m^{-3}, exhibiting a significant positive correlation with OC (y = 0.35x + 1.73, R^2 = 0.56, P < 0.01; Supplementary Data Fig. S1). WSOC contributed slightly more than the water-insoluble organic carbon to the TSP, with contributions of 5.56% and 5.02%, respectively.

TSP, OC, and EC concentrations exhibited similar seasonal variation over the 3 years, with concentrations peaking during the pre-monsoon season (particularly in April and May) and gradually decreasing to minima around the middle of the monsoon season; moderate values were maintained through the post-monsoon and winter seasons (Fig. 2). These seasonal variations were similar to the aerosol mass (PM_1 and $PM_{1\text{-}10}$) and BC concentrations at the Nepal Climate Observatory–Pyramid (NCO-P; 5079 m, southern Himalayas; March 2006 to February 2008; Marinoni et al., 2010)

Table 1
Comparison of TSP, OC, and EC concentrations (μg m^{-3}) and OC/EC ratios of aerosols in Jomsom with other sites.

Site	Particle type and method	Sampling period	OC	EC	OC/EC	TSP
Jomsom	TSP/TOR	Apr 2012 – Apr 2014 Nov 2017 – Aug 2018	9.74	2.02	5.08	92.0
Kathmandu[a]	TSP/TOR	Apr 2012 – Jan 2016	34.80	9.97	3.65	238.2
Delhi[b]	PM10/TOT	2010	26.70	6.10	4.38	511.1
Kanpur[c]	TSP/TOT	2004	25.00	4.80	6.20	
Karachi[a]	TSP/TOR	Feb 2015 – Mar 2017	39.90	8.52	4.20	
Dushanbe[d]	TSP/TOR	Sep 2018 – Aug 2019	11.90	5.13	2.30	
Lumbini[e]	TSP/TOR	Apr 2013 – Mar 2014	32.80	5.95	5.16	161.1
Manora Peak[f]	TSP/TOT	Feb 2005 – Jul 2008	8.20	1.30	7.30	68.5
Dhunche[a]	TSP/TOR	Apr 2013 – Mar 2015	14.80	3.06	5.00	
NCO-P[g]	PM_{10}/TOT	Pre-monsoon 2006–2008	2.40	0.50	4.80	
		Monsoon	0.90	0.10	9.00	
		Post-monsoon	1.40	0.10	14.00	
		Winter	1.20	0.10	12.00	
QOMS[h]	TSP/TOR	Aug 2009 – Jul 2010	1.43	0.25	6.69	
Nam Co[a]	TSP/TOR	Jul 2013- Dec 2016	1.63	0.13	8.13	

Notes: [a] – Chen et al., 2019; [b] – Sharma et al., 2014 and Chelani et al., 2010; [c] – Ram and Sarin, 2010; [d] – Chen et al., 2021; [e] – Wan et al., 2017; [f] – Ram et al., 2010; [g] – Decesari et al., 2010; [h] – Cong et al., 2015.

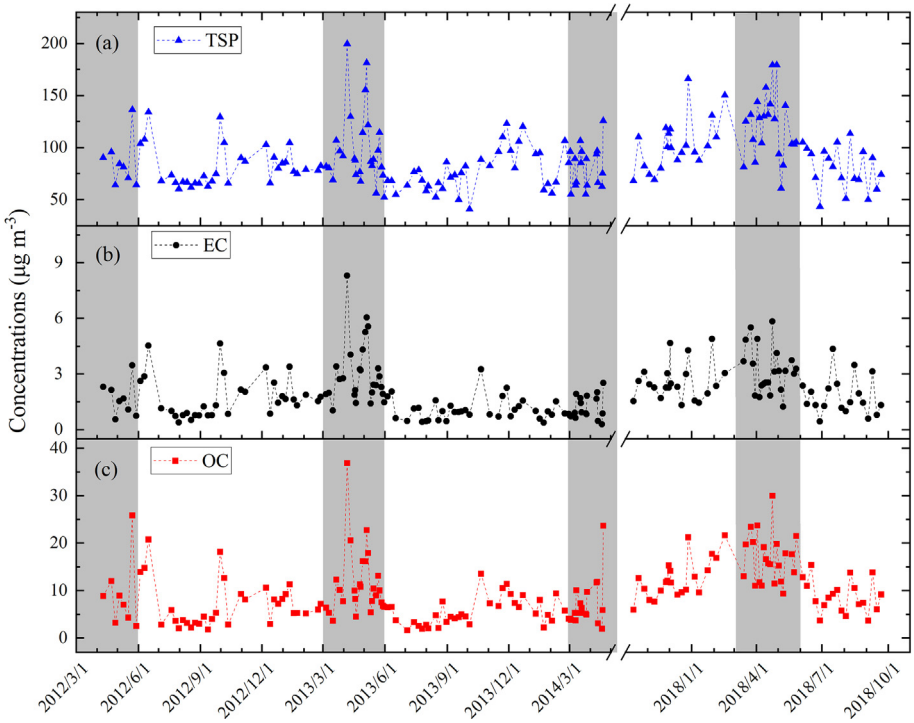

Fig. 2. Temporal variability in the abundance (μg m^{-3}) of TSP, OC, and EC during the sampling period in Jomsom. Grey rectangles cover the pre-monsoon period.

and another study of BC in Jomsom (January 2013 to July 2015) (Dhungel et al., 2018).

The concentrations of TSP and CA were significantly lower than those recorded in upwind urban or rural areas, including Kathmandu (Nepal), Delhi (India), Kanpur (India), Karachi (Pakistan), and Lumbini (Nepal), and comparable to those recorded at other remote sites, such as Manora Peak (India) and Dhunche (Nepal) in the central Himalayas (Chelani et al., 2010; Ram and Sarin, 2010; Ram et al., 2010; Sharma et al., 2014; Wan et al., 2017; Chen et al., 2020a,b). However, the OC and EC concentrations in Jomsom were approximately 6 and 10 times higher than those at the NCO-P in the foothills of Mount Everest and also higher than other remote sites inland of the Tibetan Plateau, such as the Qomolangma Station and Nam Co (Decesari et al., 2010; Cong et al., 2015; Chen et al., 2019). Located on the south slope of the Himalayas, Jomsom is a small town with few local emissions and lower pollutant concentrations than those in the upwind urban areas. However, its proximity to the heavily populated areas of IGP may results in higher pollutant levels in Jomson than in other high-altitude sites over the central Himalayas and inland of the Tibetan Plateau.

3.2. Source apportionment of EC based on $\Delta^{14}C$

The $\Delta^{14}C$ content of EC provides a direct quantitative measure of the relative contributions from fossil fuel combustion and biomass burning emissions. $\Delta^{14}C$ exhibited pronounced temporal variation, ranging from − 602‰ to − 132‰ (−375‰ ± 138‰) in Jomsom. Radiocarbon analysis revealed that the annual mean contribution of fossil fuel combustion (f_{fossil}) to EC in Jomsom was

47.9% ± 11.5%, indicating that contemporary carbon sources (biogenic and biomass combustion) and fossil fuel combustion contribute equally to EC in Jomsom. This result was outside the range generally observed in East Asia (Chen et al., 2013; Andersson et al., 2015; Fang et al., 2018). However, it was more consistent with observations in South Asia. For instance, the year-round observational-based ^{14}C-constrained source apportionment results with f_{fossil} = 47% ± 9% and f_{fossil} = 49% ± 8% were reported at the Maldives Climate Observatory at Hanimaadhoo (MCOH) and Sinhagad in India (Budhavant et al., 2015). Other studies conducted at these two South Asian sites have recorded similar fossil fuel contributions to EC. Gustafsson et al. (2009) reported f_{fossil} values of 54% ± 8% and 46% ± 2% for the MCOH and Sinhagad, respectively. Bosch et al. (2014) observed a mean f_{fossil} value of 41% ± 4% at the MCOH. A remarkable similarity in contributions of biomass burning (f_{bio}) and fossil combustion was observed at the Bangladesh Climate Observatory at Bhola (BCOB) with f_{bio} value of 50% ± 3% in the pre-monsoon season (Dasari et al., 2020). The lower f_{fossil} observed at the MCOH revealed a large divergence in the fossil fuel contributions to EC, likely attributable to the different source regions. Much higher f_{fossil} value (83%) was observed over Delhi in summer while it decreased to approximately 57% in winter (Bikkina et al., 2019). Nevertheless, most studies have reported similar contributions of fossil fuel combustion to EC, with a mean f_{fossil} value of 50% ± 6% that demonstrates good agreement with the current study. This indicated that EC in Jomsom has similar source attributions to those of the large and highly polluted IGP (Fig. 3).

$\Delta^{14}C_{EC}$ exhibited strong seasonal variability, with the highest contemporary signal observed during the winter (f_{fossil} = 38.7% ± 13.3%), followed by the pre-monsoon (f_{fossil} = 42.5% ± 6.09%), post-monsoon (f_{fossil} = 46.4% ± 1.04%), and monsoon (f_{fossil} = 59.8% ± 6.08%) seasons (Fig. 3). The seasonal variation was similar with studies conducted at other regions (e.g., Delhi, MCOH, and Sinhagad) in South Asia although with a divergence in f_{fossil} (Budhavant et al., 2015; Bikkina et al., 2019). Although the EC concentration in Jomsom was low, the fossil fuel combustion contribution falls within the range reported for South Asia during the pre-monsoon and post-monsoon seasons (Bosch et al., 2014; Budhavant et al., 2015; Gustafsson et al., 2009). Several samples collected at upwind Lumbini and Pokhara revealed similar f_{fossil} values for the pre-monsoon and post-monsoon seasons, suggesting that Jomsom predominantly receives pollutants from those regions (Li et al., 2016a). The burning of the residue of two crops (rice, October–November; wheat, April–May) over the IGP contributes approximately 21% of EC (59 ± 2 Gg y^{-1}) (Rajput et al., 2014). In addition, forest fires are potential contributors to EC in the atmosphere. Studies have reported the influence of intense haze in the IGP on Himalayan regions during dry periods (Kumar et al., 2011; Sinha et al., 2014; Ram and Sarin, 2015; Bikkina et al., 2016). Dense fire spots (representing agricultural burning and forest fires) were identified in the IGP during the non-monsoon seasons, particularly in the pre-monsoon and winter seasons (Supplementary Data Fig. S2), leading to an increase of pollutants over the IGP and to some extent to higher CA concentrations in Jomsom through long-range transport.

The lowest f_{fossil} (27.7%) was observed in winter and was lower than that reported in most regions in South Asia (Gustafsson et al., 2009; Budhavant et al., 2015; Li et al., 2016a; Bikkina et al., 2019) but similar to that reported by one study conducted in Sinhagad (Sheesley et al., 2012). Crop residue burning decreases in winter (Srinivas and Sarin, 2014); however, an increase in wood burning may contribute to the larger contribution of f_{bio} (Venkataraman et al., 2005; Gustafsson et al., 2009). In addition, more biomass is burned by local residents for heating in cold conditions, and this increase may be another reason for the higher f_{bio}. Therefore, the f_{bio} value (72.3%) of EC being highest in winter to a large extent reflects the contributions from local sources (e.g., wood burning). Furthermore, strong correlations (R^2 > 0.70) were observed between OC and EC during all seasons except winter (Supplementary Data Fig. S3). The lower correlations in winter indicated other influences (e.g., biomass burning from local activities). By contrast, the decrease of biomass burning emissions combined with intense rainfall could explain why the highest f_{fossil} was observed during the monsoon season (Dumka et al., 2010; Sarangi et al., 2014). Two samples had f_{fossil} of 66.9% and 62.8% in Jomsom, indicating major fossil fuel contributions (Fig. 3). In Kathmandu and Dhunche, Li et al. (2016a) recorded the highest f_{fossil} for EC during the monsoon season also. The f_{fossil} values were also consistent with the OC/EC ratio, which reflects the emission source variability and processing during long-range transport. For instance, the highest (5.62 ± 2.35) and lowest (4.88 ± 1.69) mean OC/EC ratios were

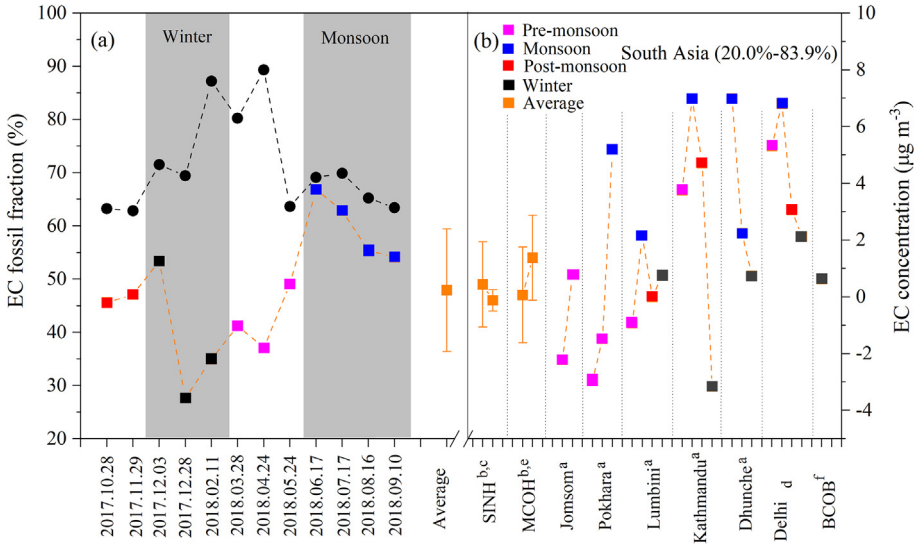

Fig. 3. Seasonal source apportionment based on 12-month continuous ^{14}C–EC observations for Jomsom and previous results from South Asia (a, Li et al., 2016a; b, Budhavant et al., 2015; c, Gustafsson et al., 2009; d, Bikkina et al., 2019; e, Bosch et al., 2014; f, Dasari et al., 2020). Black circle denotes EC concentrations and square with different colors denotes fraction of fossil fuel combustion in different seasons.

observed in the winter and monsoon seasons, respectively, corresponding with the lowest and highest f_{fossil} values observed during these two periods. The mean OC/EC ratio (5.08 ± 1.77) was similar to that reported for urban areas in the IGP, including Delhi and Lumbini (Sharma et al., 2014; Wan et al., 2017), further indicating the polluted IGP as the potential source region for the CA over Jomsom.

These year-round ^{14}C-based EC source apportionments demonstrated considerable seasonal variation in the fossil fuel combustion contribution to EC in Jomsom. This variation was similar to that in urban and rural regions of Nepal, such as Lumbini, Pokhara, and Kathmandu. However, a much lower f_{fossil} value was observed in Jomsom in winter than was observed in southern urban areas, probably indicating the influence of local biomass burning. Overall, the mean f_{fossil} in Jomsom reflects an approximately equal contribution of fossil fuel combustion to that of biomass combustion and the high-aerosol products of the IGP spreading over South Asia (Lawrence and Lelieveld, 2010; Sheesley et al., 2012; Kirillova et al., 2014; Li et al., 2016a). The isotope-based source apportionment results validate previous theories that EC aerosols from the IGP can be transported to the Himalayas.

3.3. Air mass transport analysis

To more fully understand the atmospheric conditions and transport pathways of EC in different seasons in Jomsom, 5-day air mass back trajectories (500 m above the ground) obtained from the National Oceanic and Atmospheric Administration's HYSPLIT4 model, together with an active fire map generated using the National Aeronautics and Space Administration moderate-resolution imaging spectroradiometer (MODIS), were calculated (Supplementary Data Fig. S2). The air mass reaching Jomsom was consistent with the circulation patterns reported by Tripathee et al. (2017). During the monsoon season, air masses arrived from two main directions; more than half of the air masses originated from the southeast, possibly passing through metropolitan areas such as Kathmandu and conveying air moisture from the Bay of Bengal. The other air masses originated from the IGP, which harbors air pollutants from several sources. During the non-monsoon seasons, strong westerlies pass through western Nepal, northwestern India, and Pakistan.

The transport pathways of the air masses arriving in Jomsom during the non-monsoon seasons were similar; however, a distinctly higher CA level was recorded in the pre-monsoon season (Fig. 2), emphasizing the influence of source strength changes. As previously reported, pollutant concentrations along the Himalayas are partly affected by open fire emissions (Bonasoni et al., 2008; Kumar et al., 2011; Ram and Sarin, 2015). The densest fire spots were detected in the pre-monsoon season (Supplementary Data Fig. S2), likely leading the high OC and EC concentrations during these periods. However, OC and EC concentrations were considerably lower in winter than in the pre-monsoon season, despite similar incidence of open fires, indicating that Jomsom receives the synthetic contributions from fossil fuel and biomass burning in surrounding regions, particularly Nepal and the IGP.

In addition to the large-scale air mass transport, a diurnal valley wind system caused by local orographic conditions and temperature differences is created between the mountaintops and lowlands, with daytime up-valley winds switching to down-valley winds during the night. The southerly up-valley winds reach maximum speeds in the afternoon and are capable of delivering air pollutants from the foothills to higher altitudes (Bonasoni et al., 2008). Further consultation of the Cloud-Aerosol Lidar with Orthogonal Polarization data for April 29, 2013, provided an aerosol vertical profile (Supplementary Data Fig. S4) representative of high-aerosol-loading days within the sampling period. The data reveal that the pollution plume reaches approximately 3 km on that day, sufficient to reach the sampling site. Additionally, CWT analysis was performed for EC. The results further indicated that major contributions were made to EC by air masses passing through the northern IGP in the non-monsoon seasons, and the easterly wind originating from the Bay of Bengal during the monsoon season is another non-negligible source (Supplementary Data Fig. S5). However, the diurnal valley wind system was not well demarcated in the present study. The air mass transport analysis provided indirect evidence to trace the source regions but it cannot identify the influence of local emission which was mainly controlled by regional wind system.

3.4. Light absorption properties of EC and WSOC

It is essential to know the MAC of light absorbing particles which is generally used to evaluate the radiative forcing. The MAC_{EC} in Jomsom ranged from 3.42 to 13.1 m^2/g, with a mean value of 8.27 ± 1.76 m^2/g for the sampling period. Employing the method developed by Cheng et al. (2011), we compared the observed data with equivalent MAC data from other sites (Fig. 4). The MAC_{EC} value we observed in Jomsom was higher than those of urban and rural regions, such as Kanpur (Choudhary et al., 2018), Lumbini, and Pokhara, and similar to those at remote sites (e.g., Dhunche and Everest) in the central Himalayas (Chen et al., 2019). However, it was significantly lower than those inland of the Tibetan Plateau (Li et al., 2016b; Chen et al., 2019). Emission sources and coating enhancement are key factors influencing MAC_{EC} (Chen and Bond, 2010; Gustafsson and Ramanathan, 2016; Peng et al., 2016; Hu et al., 2017). The equivalent MAC was lower in urban areas of South Asia because such regions are largely affected by local emissions and particles undergoing minor aging processes. The slightly higher MAC_{EC} values in Jomsom indicated that it is affected by long-range pollutant transport.

Clear seasonal variation of MAC_{EC} was observed in Jomsom, with the highest value recorded in the monsoon season, moderate values in the pre-monsoon and post-monsoon seasons, and the lowest value in winter (Fig. 5). Similar trends have been reported in other locations such as Manora Peak, Lumbini, and Beijing (Ram et al., 2010; Cheng et al., 2011; Chen et al., 2020b). The slightly higher MAC_{EC} values observed during the monsoon season were attributable to the greater coating of EC with secondary aerosols or other chemicals (Bond and Bergstrom, 2006; Moffet and Prather, 2009; Gustafsson and Ramanathan, 2016; Peng et al., 2016). A positive correlation between MAC_{EC} values and OC/EC ratios (Supplementary Data Fig. S6, $y = 0.43x + 1.29$, $R^2 = 0.51$, $P < 0.01$) was observed in this study, indicating that secondary OC (SOC) plays a vital role in MAC_{EC}. Correspondingly, biomass burning reduces MAC_{EC} values (Cheng et al., 2011; Hu et al., 2017). Regarding the non-monsoon seasons, crop residue burning contributed significantly to the EC in the atmosphere, resulting in a low MAC_{EC}.

Multiple scattering correction factor is one of the most uncertain parameters when retrieving the aerosol light absorption coefficient (Kim et al., 2019). For instance, a value of 2.14 has been suggested for correction due to the multiple scattering effect for uncoated and externally mixed soot particles collected on tissue quartz filters. Several other values (e.g., 2.23 ± 0.79; 2.29 ± 1.36) were suggested for various situation (Weingartner et al., 2003; Kim et al., 2019). The sampling site was far away from Jomsom town thus we think the atmosphere is mixture with most parts from long-range transport air mass and few from local emission. Therefore, we used the value of 3.6 which was determined during experiments for internally mixed aerosols (e.g., soot particles coated with organics; Ram and Sarin, 2009). This value was also used in remote Himalayan regions such as Manora Peak (Ram

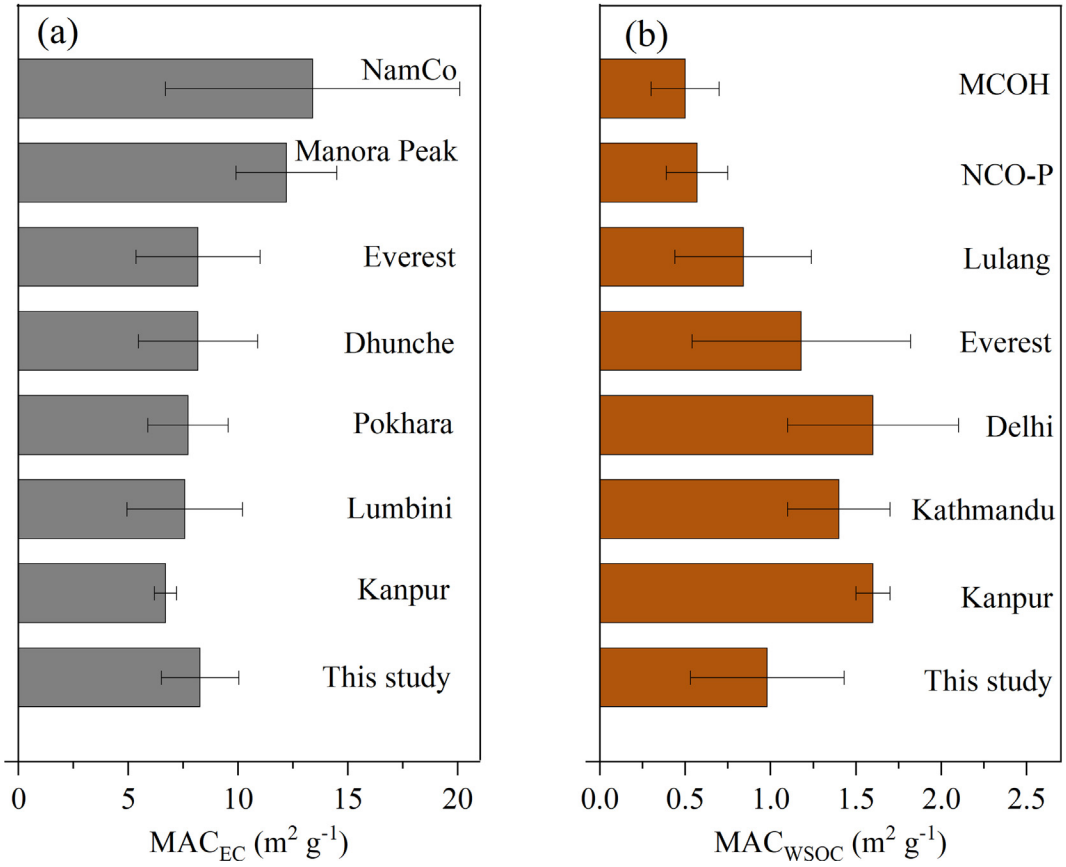

Fig. 4. MAC values (m^2/g) of EC and WSOC in Jomsom compared with those in other regions. (Kanpur: PM_1 samples, Choudhary et al., 2018; Lumbini, Pokhara, Dhunche, Everest, and Nam Co: TSP samples, Chen et al., 2019; Kathmandu: TSP samples, Chen et al., 2020c; Manora Peak: TSP samples, Ram et al., 2010; MCOH: TSP and $PM_{2.5}$ samples at Maldives Climate Observatory on Hanimaadhoo, Bosch et al., 2014; Delhi: PM_{10} samples, Kirillova et al., 2014; NCO-P: PM_{10} samples, Kirillova et al., 2016; Lulang: TSP samples, Li et al., 2016b).

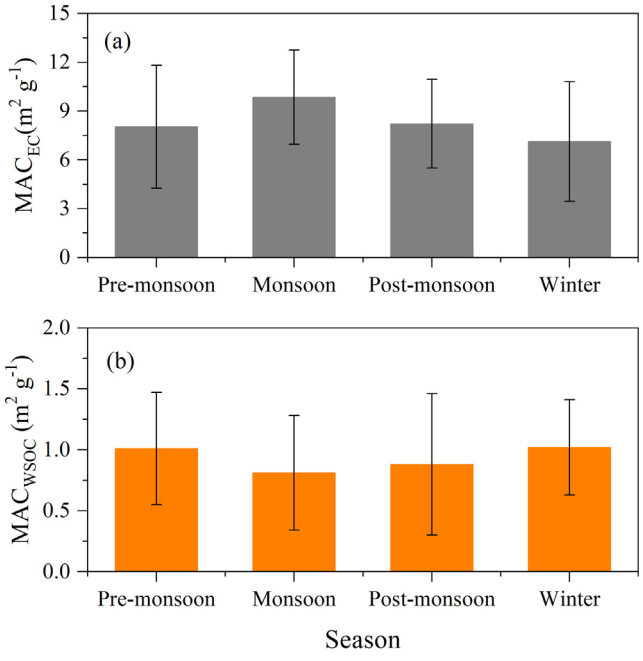

Fig. 5. Seasonal variations in MAC values (m^2/g) of EC and WSOC in Jomsom.

et al., 2010) and Everest (Li et al., 2016b). However, this study didn't give any information about EC morphology and coating thus the calculation has uncertainties.

The mean MAC_{WSOC} value at 365 nm was 0.98 ± 0.45 m^2/g for the TSP in Jomsom, which is lower than those of typical urban areas heavily influenced by local combustion emissions from South Asia (e.g., Delhi: 1.60 ± 0.45 m^2/g, Kirillova et al., 2014b; BCOB: 1.4 ± 0.2 m^2/g, Dasari et al., 2019) but higher than those at remote sites, such as the NCO-P and regions inland of the Tibetan Plateau (Kirillova et al., 2016). The photobleaching of WSOC during transport is likely the main factor causing such spatial distribution (Forrister et al., 2015). Slightly higher MAC_{WSOC} was observed during the winter and pre-monsoon seasons (Fig. 5), possibly due to the WSOC originating from multiple sources of absorbing species (e.g., biomass burning) and fine particles being entrained from surface soil (Li et al., 2021). The MAC_{WSOC} decreased in the monsoon season, indicating a strong intensive washing-out effect of WSOC or an increased SOC contribution because of high humidity and temperature (Saleh et al., 2013).

An absorption-based method was used to calculate the relative light absorptive contribution of WSOC to EC (f_{WSOC}) in Jomsom. The f_{WSOC} value ranged from 2.54% to 18.7% with an average of 11.1% ± 4.23%. The result was comparable to those reported for severely polluted Delhi in the IGP (3%–11%), the East Asian outflow (2%–10%) (Kirillova et al., 2014a, b), and the Everest station (11.41% ± 7.08%) on the north slope of the Himalayas (Li et al., 2016b).

However, the f_{WSOC} values were significantly higher than those for remote regions, such as for the South Asian outflow at the MCOH in the Indian Ocean (0.7% ± 0.2%) (Bosch et al., 2014). The f_{WSOC} indicated that WSOC contributed a large fraction of the light absorption compared with EC, although in various locations surrounding the Himalayas. Thus, studying EC and WSOC together reduces the uncertainty in the estimation of atmospheric radiative forcing due to CA.

3.5. Implications

Air pollution is increasing rapidly in South Asia particularly in the IGP. Modeling work have predicted high urban growth in northwestern part of this region. While in other parts, the growth concentrated around several big cities such as Kolkata, Jharkhand, and Delhi (Chowdhury and Maithani, 2014; Verma et al., 2022). Apart from urban growth, seasonal crop residue burning activities in rural areas significantly affect the air quality of the IGP. These activities could lead to severe air pollution episodes during the non-monsoon season (Bikkina et al., 2019; Ravindra et al., 2021; Lin and Begho, 2022).

The prevalent air pollution over the IGP indicate major contributions from biofuel and crop burning as well as fossil fuel combustion. Model-simulated and source-diagnostic ground-based observations have determined that polluted air masses can reach and cross the high mountain range through the major north–south valleys and by being lifted and advected over the Greater Himalayas (Lüthi et al., 2015; Li et al., 2016a; Yang et al., 2018; Gong et al., 2019). This study provides evidence of the transport of EC from the IGP and Nepal to the higher Himalayas. The $\Delta^{14}C$ fingerprints assisted in determining the sources of the EC over Jomsom, revealing the approximately equal influence of biomass and fossil fuel combustion sources to the southern Himalaya; the same source division/fingerprint as in the IGP emission source region (e.g., Kirillova et al., 2014a, b; Bikkina et al., 2019; Dasari et al., 2020; Salam et al., 2021). However, these mass- and duration-weighted annual averages revealed a divergence in the biomass contributions to EC. The back-trajectory analysis indicated that differences in source regions may explain the differences in the EC biomass contributions of the monsoon and non-monsoon seasons. In addition, increased local burning activities in winter result in higher f_{bio}. Large-scale air circulation plays a key role in the accumulation of pollutants on the south slope of the Himalayas. In addition, local meteorological patterns, including updrafts near heated mountain flanks and valley wind systems, accelerate the spread of pollutants up the mountains and across the widely distributed valleys (Bonasoni et al., 2008; Dhungel et al., 2018).

Over 30 valleys cross the Himalayan Mountain range from the IGP, essentially serving as channels for pollutants to reach the vulnerable southern slope of the Himalayas (Gong et al., 2019). EC can prevent solar radiation from reaching the surface and interfere with cloud formation and precipitation, threating the climate of the region. Additionally, EC and BrC have cumulative effects that accelerate the melting of glaciers and thus affect the delivery of valuable water resources (Xu et al., 2009; Zhang et al., 2017; Kang et al., 2019). Long-term campaigns are crucial to alleviate the deficit of observational constraints of predictions based on emissions inventory estimates. Such observation-based source apportionment of EC facilitates reliability on modeling of the climatic and hydrological effects of EC in the Himalayas and guide policy-making aimed at mitigating emissions. However, long-term ground-based observation is largely lacking in such large mountainous areas. Further observation and modeling studies are therefore urgently required to identify the chemical speciation and spatiotemporal distribution of pollutants in the Himalayas to ascertain their climatic and environmental implications.

4. Conclusion

TSP samples were collected from April 2012 to March 2014 and October 2017 to September 2018 at Jomsom, a high-altitude site in the central Himalayas, to analyze CA concentration and its light absorption characteristic. In addition, f_{fossil} of EC was investigated. The annual mean TSP, OC, and EC concentrations were 92.0 ± 28.6, 9.74 ± 6.31, and 2.02 ± 1.35 μg m^{-3}, respectively. Most components showed the highest concentrations during the pre-monsoon season, followed by the post-monsoon, winter, and monsoon seasons, which was mainly controlled by variation of emission source and meteorological condition. Mean f_{fossil} to EC was 47.9% ± 11.5%, with the lowest (38.7% ± 13.3%) and highest (59.8% ± 6.08%) contribution appeared during winter and monsoon seasons, respectively. The result was consistent with the observation conducted at urban and remote regions in South Asia, suggesting Jomsom was mainly influenced by long-range transport pollutants from upwind regions. In addition, local biomass burning likely contributed to some extent in winter. The MAC_{EC} (8.27 ± 1.76 m^2/g) was higher than that of fresh particles, while the mean MAC_{WSOC} at 365 nm (0.98 ± 0.45 m^2/g) was lower than that in upwind regions, further suggesting that particles were mainly sourced from long-range transport. The seasonal variations of MAC of EC and WSOC were somewhat affected by coating, photobleaching processes and biomass burning. WSOC has a significant light absorption and contributes about one tenth of that of EC (11.1% ± 4.23%). Pollutants of light absorbing particles reaching this region could accelerate glacier melting and thus affect water resource for billions of people. Therefore, further studies are urgently needed to identify the pollutant status in the Himalayas.

Declaration of Competing Interest

The authors declare that they have no known competing financial interests or personal relationships that could have appeared to influence the work reported in this paper.

Acknowledgments

This study was supported by the Second Tibetan Plateau Scientific Expedition and Research Program (STEP) (2019QZKK0605), Pan-Third Pole Environment Study for a Green Silk Road (Pan-TPE) (XDA20040501), the National Natural Science Foundation of China (41705132, 41630754), the State Key Laboratory of Cryospheric Science (SKLCS-ZZ-2022), the Asia-Pacific Network for Global Change Research (APN) (CRECS2020-07MY-Tripathee) as well as the Swedish Research Council VR Distinguished Professorship grant to Ö. Gustafsson (no. 2017-01601). This study is a part of a framework spanning the Himalayas and the Tibetan Plateau: Atmospheric Pollution and Cryospheric Change (APCC). The authors acknowledge the invaluable assistance of the staff at the Jomsom sampling site. This manuscript was edited by Wallace Academic Editing.

Appendix A. Supplementary data

Supplementary data to this article can be found online at https://doi.org/10.1016/j.gsf.2022.101516.

References

Alexander, D.T.L., Crozier, P.A., Anderson, J.R., 2008. Brown carbon spheres in East Asian outflow and their optical properties. Science 321 (5890), 833–836.
Andersson, A., Deng, J.J., Du, K., Zheng, M., Yan, C.Q., Skold, M., Gustafsson, Ö., 2015. Regionally-varying combustion sources of the January 2013 severe haze events over eastern China. Environ. Sci. Technol. 49 (4), 2038–2043.

Bahadur, R., Praveen, P.S., Xu, Y., Ramanathan, V., 2012. Solar absorption by elemental and brown carbon determined from spectral observations. Proc. Natl. Acad. Sci. U.S.A. 109 (43), 17366–17371.
Bikkina, S., Andersson, A., Sarin, M.M., Sheesley, R.J., Kirillova, E., Rengarajan, R., Sudheer, A.K., Ram, K., Gustafsson, Ö., 2016. Dual carbon isotope characterization of total organic carbon in wintertime carbonaceous aerosols from northern India. J. Geophys. Res. Atmos. 121 (9), 4797–4809.
Bikkina, S., Andersson, A., Kirillova, E.N., Holmstrand, A., Tiwari, S., Srivastava, A.K., Bisht, D.S., Gustafsson, Ö., 2019. Air quality in megacity Delhi affected by countryside biomass burning. Nat. Sustain. 2 (3), 200–205.
Birch, M.E., Cary, R.A., 1996. Elemental carbon-based method for monitoring occupational exposures to particulate diesel exhaust. Aerosol. Sci. Technol. 25 (3), 221–241.
Bonasoni, P., Laj, P., Angelini, F., Arduini, J., Bonafe, U., Calzolari, F., Cristofanelli, P., Decesari, S., Facchini, M.C., Fuzzi, S., Gobbi, G.P., Maione, M., Marinoni, A., Petzold, A., Roccato, F., Reger, J.C., Sellegri, K., Sprenger, M., Venzac, H., Verza, G. P., Villani, P., Vuillermoz, E., 2008. The ABC-Pyramid Atmospheric Research Observatory in Himalayas for aerosol, ozone and halocarbon measurements. Sci. Total. Environ. 391 (2–3), 252–261.
Bond, T.C., Bergstrom, R.W., 2006. Light absorption by carbonaceous particles: an investigative review. Aerosol. Sci. Technol. 40 (1), 27–67.
Bond, T.C., Doherty, S.J., Fahey, D.W., Forster, P.M., Berntsen, T., DeAngelo, B.J., Flanner, M.G., Ghan, S., Karcher, B., Koch, D., Kinne, S., Kondo, Y., Quinn, P.K., Sarofim, M.C., Schultz, M.G., Schulz, M., Venkataraman, C., Zhang, H., Zhang, S., Bellouin, N., Guttikunda, S.K., Hopke, P.K., Jacobson, M.Z., Kaiser, J.W., Klimont, Z., Lohmann, U., Schwarz, J.P., Shindell, D., Storelvmo, T., Warren, S.G., Zender, C. S., 2013. Bounding the role of black carbon in the climate system: A scientific assessment. J. Geophysi. Res. Atmos. 118 (11), 5380–5552.
Bosch, C., Andersson, A., Kirillova, E.N., Budhavant, K., Tiwari, S., Praveen, P.S., Russell, L.M., Beres, N.D., Ramanathan, V., Gustafsson, Ö., 2014. Source-diagnostic dual-isotope composition and optical properties of water-soluble organic carbon and elemental carbon in the South Asian outflow intercepted over the Indian Ocean. J. Geophys. Res. Atmos. 119 (20), 11743–11759.
Budhavant, K., Andersson, A., Bosch, C., Krusa, M., Kirillova, E.N., Sheesley, R.J., Safai, P.D., Rao, P.S.P., Gustafsson, Ö., 2015. Radiocarbon-based source apportionment of elemental carbon aerosols at two South Asian receptor observatories over a full annual cycle. Environ. Res. Lett. 10, (6). https://doi.org/10.1088/1748-9326/10/6/064004 064004.
Cao, J.J., Lee, S.C., Ho, K.F., Zhang, X.Y., Zou, S.C., Fung, K., Chow, J.C., Watson, J.G., 2003. Characteristics of carbonaceous aerosol in Pearl River Delta Region, China during 2001 winter period. Atmos. Environ. 37 (11), 1451–1460.
Chelani, A.B., Gajghate, D.G., ChalapatiRao, C.V., Devotta, S., 2010. Particle size distribution in ambient air of Delhi and its statistical analysis. Bull. Environ. Contam. Toxicol. 85 (1), 22–27.
Chen, B., Andersson, A., Lee, M., Kirillova, E.N., Xiao, Q.F., Krusa, M., Shi, M.N., Hu, K., Lu, Z.F., Streets, D.G., Du, K., Gustafsson, Ö., 2013. Source forensics of black carbon aerosols from China. Environ. Sci. Technol. 47 (16), 9102–9108.
Chen, Y., Bond, T.C., 2010. Light absorption by organic carbon from wood combustion. Atmos. Chem. Phys. 10 (4), 1773–1787.
Chen, P.F., Kang, S.C., Li, C.L., Zhang, Q.G., Guo, J.M., Tripathee, L., Zhang, Y.L., Li, G., Gul, C., Cong, Z.Y., Wan, X., Niu, H.W., Panday, A.K., Rupakheti, M., Ji, Z.M., 2019. Carbonaceous aerosol characteristics on the Third Pole: A primary study based on the Atmospheric Pollution and Cryospheric Change (APCC) network. Environ. Pollut. 253, 49–60.
Chen, P.F., Kang, S.C., Gul, C., Tripathee, L., Wang, X.X., Hu, Z.F., Li, C.L., Pu, T., 2020a. Seasonality of carbonaceous aerosol composition and light absorption properties in Karachi. Pakistan. J. Environ. Sci. 90, 286–296.
Chen, P.F., Kang, S.C., Tripatheea, L., Panday, A.K., Rupakheti, M., Rupakheti, D., Zhang, Q.G., Guo, J.M., Li, C.L., Pu, P., 2020b. Severe air pollution and characteristics of light-absorbing particles in a typical rural area of the Indo-Gangetic Plain. Environ. Sci. Pollut. Res. 27 (10), 10617–10628.
Chen, P.F., Kang, S.C., Tripathee, L., Ram, K., Rupakheti, M., Panday, A.K., Zhang, Q.G., Guo, J.M., Wang, X.X., Pu, T., Li, C.L., 2020c. Light absorption properties of elemental carbon (EC) and water-soluble brown carbon (WS-BrC) in the Kathmandu Valley, Nepal: A 5-year study. Environ. Pollut. 261,. https://doi.org/10.1016/j.envpol.2020.114239 114239.
Chen, P.F., Kang, S.C., Abdullaev, S., Safarov, M.S., Huang, J., Hu, Z.F., Tripathee, L., Li, C.L., 2021. Significant influence of carbonates on determining organic carbon and black carbon: a case study in Tajikistan. Central Asia. Environ. Sci. Technol. 55 (5), 2839–2846.
Cheng, Y., He, K.B., Zheng, M., Duan, F.K., Du, Z.Y., Ma, Y.L., Tan, J.H., Yang, F.M., Liu, J. M., Zhang, X.L., Weber, R.J., Bergin, M.H., Russell, A.G., 2011. Mass absorption efficiency of elemental carbon and water-soluble organic carbon in Beijing. China. Atmos. Chem. Phys. 11 (22), 11497–11510.
Choudhary, V., Rajput, P., Singh, D.K., Singh, A.K., Gupta, T., 2018. Light absorption characteristics of brown carbon during foggy and non-foggy episodes over the Indo-Gangetic Plain. Atmos. Pollut. Res. 9 (3), 494–501.
Chow, J.C., Watson, J.G., Chen, L.W.A., Chang, M.C.O., Robinson, N.F., Trimble, D., Kohl, S., 2007. The IMPROVE-A temperature protocol for thermal/optical carbon analysis: maintaining consistency with a long-term database. J. Air. Waste. Manage. Assoc. 57 (9), 1014–1023.
Chowdhury, P.K.R., Maithani, S., 2014. Modelling urban growth in the Indo-Gangetic plain using nighttime OLS data and cellular automata. Int. J. Appl. Earth. Obs. 33, 155–165.
Chung, C.E., Ramanathan, V., Decremera, D., 2012. Observationally constrained estimates of carbonaceous aerosol radiative forcing. Proc. Natl. Acad. Sci. U.S.A. 109 (19), 11624–11629.
Cong, Z., Kang, S., Kawamura, K., Liu, B., Wan, X., Wang, Z., Gao, S., Fu, P., 2015. Carbonaceous aerosols on the south edge of the Tibetan Plateau: concentrations, seasonality and sources. Atmos. Chem. Phys. 15 (3), 1573–1584.
Dasari, S., Andersson, A., Bikkina, S., Holmstrand, H., Budhavant, K., Satheesh, S., Asmi, E., Kesti, J., Backman, J., Salam, A., Bisht, D.S., Tiwari, S., Hameed, Z., Gustafsson, Ö., 2019. Photochemical degradation affects the light absorption of water-soluble brown carbon in the South Asian outflow. Sci. Adv. 5, eaau8066. https://doi.org/10.1126/sciadv.aau8066.
Dasari, S., Andersson, A., Stohl, A., Evangeliou, N., Bikkina, S., Holmstrand, H., Budhavant, K., Salam, A., Gustafsson, Ö., 2020. Source quantification of South Asian black carbon aerosols with isotopes and modeling. Environ. Sci. Technol. 54 (19), 11771–11779.
Decesari, S., Facchini, M.C., Carbone, C., Giulianelli, L., Rinaldi, M., Finessi, E., Fuzzi, S., Marinoni, A., Cristofanelli, P., Duchi, R., Bonasoni, P., Vuillermoz, E., Cozic, J., Jaffrezo, J.L., Laj, P., 2010. Chemical composition of PM_{10} and PM_1 at the high-altitude Himalayan station Nepal Climate Observatory-Pyramid (NCO-P) (5079 m a.s.l.). Atmos. Chem. Phys. 10 (10), 4583–4596.
Dhungel, S., Kathayat, B., Mahata, K., Panday, A., 2018. Transport of regional pollutants through a remote trans-Himalayan valley in Nepal. Atmos. Chem. Phys. 18 (2), 1203–1216.
Draxler, R.R., Rolph, G.D., 2012. HYSPLIT (Hybrid Single Particle Lagrangian Integrated Trajectory) Model access via NOAA ARL READY Website, available at: http://ready.arl.noaa.gov/HYSPLIT.Pphp, NOAA Air Resources Laboratory, Silver Spring, MD., 2012.
Dumka, U.C., Moorthy, K.K., Kumar, R., Hegde, P., Sagar, R., Pant, P., Singh, N., Babu, S. S., 2010. Characteristics of aerosol black carbon mass concentration over a high altitude location in the central Himalayas from multi-year measurements. Atmos. Res. 96 (4), 510–521.
Fang, W.Z., Du, K., Andersson, A., Xing, Z.Y., Cho, C.Y., Kim, S.W., Deng, J.J., Gustafsson, Ö., 2018. Dual-isotope constraints on seasonally resolved source fingerprinting of black carbon aerosols in sites of the four emission hot spot regions of China. J. Geophy. Res. Atmos. 123 (20), 11735–11747.
Flanner, M.G., Zender, C.S., Hess, P.G., Mahowald, N.M., Painter, T.H., Ramanathan, V., Rasch, P.J., 2009. Springtime warming and reduced snow cover from carbonaceous particles. Atmos. Chem. Phys. 9 (7), 2481–2497.
Forrister, H., Liu, J., Scheuer, E., Dibb, J., Ziemba, L., Thornhill, K.L., Anderson, B., Diskin, G., Perring, A.E., Schwarz., J.P., Campuzano-Jost, P., Day, D.A., Palm, B.B., Jimenez, J.L., Nenes, A., Weber, R.J., 2015. Evolution of brown carbon in wildfire plumes. Geophys. Res. Lett. 42(11), 4623−4630.
Gong, P., Wang, X.P., Pokhrel, B., Wang, H.L., Liu, X.D., Liu, X.B., Wania, F., 2019. Trans-Himalayan transport of organochlorine compounds: three-year observations and model-based flux estimation. Environ. Sci. Technol. 53 (12), 6773–6783.
Graven, H.D., Guilderson, T.P., Keeling, R.F., 2012. Observations of radiocarbon in CO_2 at seven global sampling sites in the Scripps flask network: analysis of spatial gradients and seasonal cycles. J. Geophys. Res. 117, D02303. https://doi.org/10.1029/2011JD016535.
Gustafsson, Ö., Krusà, M., Zencak, Z., Sheesley, R.J., Granat, L., Engström, E., Praveen, P., Rao, P., Leck, C., Rodhe, H., 2009. Brown clouds over South Asia: biomass or fossil fuel combustion? Science 323 (5913), 495–498.
Gustafsson, Ö., Ramanathan, V., 2016. Convergence on climate warming by black carbon aerosols. Proc. Natl. Acad. Sci. U.S.A. 113 (16), 4243–4245.
Hansen, J., Nazarenko, L., 2004. Soot climate forcing via snow and ice albedos. Proc. Natl. Acad. Sci. U.S.A. 101 (2), 423–428.
Hindman, E.E., Upadhyay, B.P., 2002. Air pollution transport in the Himalayas of Nepal and Tibet during the 1995–1996 dry season. Atmos. Environ. 36 (4), 727–739.
Hodnebrog, O., Myhre, G., Samset, B.H., 2014. How shorter black carbon lifetime alters its climate effect. Nat. Commun. 5, 5065. https://doi.org/10.1038/ncomms6065.
Hu, Z.F., Kang, S.C., Li, C.L., Yan, F.P., Chen, P.F., Gao, S.P., Wang, Z.Y., Zhang, Y.L., Sillanpää, M., 2017. Light absorption of biomass burning and vehicle emission-sourced carbonaceous aerosols of the Tibetan Plateau. Environ. Sci. Pollut. Res. 24 (18), 15369–15378.
Ji, Z.M., Kang, S.C., Cong, Z.Y., Zhang, Q.G., Yao, T.D., 2015. Simulation of carbonaceous aerosols over the Third Pole and adjacent regions: distribution, transportation, deposition, and climatic effects. Clim. Dyn. 45 (9–10), 2831–2846.
Kang, S.C., Zhang, Q.G., Qian, Y., Ji, Z.M., Li, C.L., Cong, Z.Y., Zhang, Y.L., Guo, J.M., Du, W.T., Huang, J., You, Q.L., Panday, A.K., Rupakheti, M., Chen, D.L., Gustafsson, Ö., Thiemens, M.H., Qin, D.H., 2019. Linking atmospheric pollution to cryospheric change in the Third Pole Region: Current progresses and future prospects. Natl. Sci. Rev. 6 (4), 796–809.
Kang, S.C., Zhang, Y.L., Qian, Y., Wang, H.L., 2020. A review of black carbon in snow and ice and its impact on the cryosphere. Earth Sci. Rev. 210,. https://doi.org/10.1016/j.earscirev.2020.103346 103346.
Kang, S.C., Zhang, Y.L., Chen, P.F., Guo, J.M., Zhang, Q.G., Cong, Z.Y., Kaspari, S., Tripathee, L., Gao, T.G., Niu, H.W., Zhong, X.Y., Chen, X.T., Hu, Z.F., Li, X.F., Li, Y., Neupane, B., Yan, F.P., Rupakheti, D., Gul, C., Zhang, W., Wu, G.M., Yang, L., Wang, Z.Q., Li, C.L., 2022. Black carbon and organic carbon dataset over the Third Pole. Earth Syst. Sci. Data. 14 (2), 683–707.

Kim, J.H., Kim, S.W., Ogren, J.A., Sheridan, P.J., Yoon, S.C., Sharma, S., Lin, N.H., 2019. Multiple scattering correction factor estimation for aethalometer aerosol absorption coefficient measurement. Aerosol Sci. Technol. 53 (2), 160–171.

Kirillova, E.N., Andersson, A., Han, J., Lee, M., Gustafsson, Ö., 2014a. Sources and light absorption of water-soluble organic carbon aerosols in the outflow from northern China. Atmos. Chem. Phys. 14 (3), 1413–1422.

Kirillova, E.N., Andersson, A., Tiwari, S., Srivastava, A.K., Bisht, D.S., Gustafsson, Ö., 2014b. Water-soluble organic carbon aerosols during a full New Delhi winter: isotope-based source apportionment and optical properties. J. Geophys. Res. Atmos. 119 (6), 3476–3485.

Kirillova, E.N., Marinoni, A., Bonasoni, P., Vuillermoz, E., Facchini, M.C., Fuzzi, S., Decesari, S., 2016. Light absorption properties of brown carbon in the high Himalayas. J. Geophys. Res. Atmos. 121 (16), 9621–9639.

Klinedinst, D.B., Currie, L.A., 1999. Direct quantification of $PM_{2.5}$ fossil and biomass carbon within the northern front range air quality study's domain. Environ. Sci. Technol. 33 (23), 4146–4154.

Kumar, R., Naja, M., Satheesh, S.K., Ojha, N., Joshi, H., Sarangi, T., Pant, P., Dumka, U. C., Hedge, P., Venkataramani, S., 2011. Influences of the springtime northern Indian biomass burning over the central Himalayas. J. Geophys. Res. Atmos. 166, D19302. https://doi.org/10.1029/2010JD015509.

Lawrence, M., Lelieveld, J., 2010. Atmospheric pollutant outflow from southern Asia: A review. Atmos. Chem. Phys. 10 (22), 11017–11096.

Li, C.L., Bosch, C., Kang, S.C., Andersson, A., Chen, P.F., Zhang, Q.G., Cong, Z.Y., Chen, B., Qin, D.H., Gustafsson, Ö., 2016a. Sources of black carbon to the Himalayan-Tibetan Plateau glaciers. Nat. Commun. 7, 12574. https://doi.org/10.1038/ncomms12574.

Li, C.L., Yan, F.P., Kang, S.C., Chen, P.F., Hu, Z.F., Gao, S.P., Qu, B., Sillanpää, M., 2016b. Light absorption characteristics of carbonaceous aerosols in two remote stations of the southern fringe of the Tibetan Plateau. China. Atmos. Environ. 143, 79–85.

Li, C.L., Yan, F.P., Kang, S.C., Yan, C.Q., Hu, Z.F., Chen, P.F., Gao, S.P., Zhang, C., He, C.L., Kaspari, S., Stubbins, A., 2021. Carbonaceous matter in the atmosphere and glaciers of the Himalayas and the Tibetan Plateau: An investigative review. Environ. Int. 146,. https://doi.org/10.1016/j.envint.2020.106281 106281.

Lin, M.Y., Begho, T., 2022. Crop residue burning in South Asia: A review of the scale, effect, and solutions with a focus on reducing reactive nitrogen losses. J. Environ. Manage. 314,. https://doi.org/10.1016/j.jenvman.2022.115104 115104.

Lüthi, Z.L., Škerlak, B., Kim, S.W., Lauer, A., Mues, A., Rupakheti, M., Kang, S.C., 2015. Atmospheric brown clouds reach the Tibetan Plateau by crossing the Himalayas. Atmos. Chem. Phys. 15 (11), 6007–6021.

Marinoni, A., Cristofanelli, P., Laj, P., Duchi, R., Calzolari, F., Decesari, S., Sellefri, K., Vuillermoz, E., Verza, G., Villani, P., Bonasoni, P., 2010. Aerosol mass and black carbon concentrations, a two year record at NCO-P (5079 m, Southern Himalayas). Atmos. Chem. Phys. 10 (17), 8551–8562.

Meehl, G., Arblaster, J., Collins, W., 2008. Effects of black carbon aerosols on the Indian monsoon. J. Climate. 21 (12), 2869–2882.

Menon, S., Hansen, J., Nazarenko, L., Luo, Y., 2002. Climate effects of black carbon aerosols in China and India. Science 297 (5590), 2250–2253.

Moffet, R.C., Prather, K.A., 2009. In-situ measurements of the mixing state and optical properties of soot with implications for radiative forcing estimates. Proc. Natl. Acad. Sci. U.S.A. 106 (29), 11872–11877.

Peng, J.F., Hu, M., Guo, S., Du, Z.F., Zheng, J., Shang, D.J., Zamora, M.L., Zeng, L.M., Shao, M., Wu, Y.S., Zheng, J., Wang, Y., Glen, C.R., Collins, D.R., Molina, M.J., Zhang, R.Y., 2016. Markedly enhanced absorption and direct radiative forcing of black carbon under polluted urban environments. Proc. Natl. Acad. Sci. U.S.A. 113 (16), 4266–4271.

Rai, M., Kang, S.C., Yang, J.H., Chen, X.T., Hu, Y.L., Rupakheti, D., 2022. Tracing atmospheric anthropogenic black carbon and its potential radiative response over Pan-Third Pole region: A synoptic-scale analysis using WRF-Chem. J. Geophys. Res. 127 (6), D035772. https://doi.org/10.1029/2021JD035772.

Rajput, P., Sarin, M., Sharma, D., Singh, D., 2014. Characteristics and emission budget of carbonaceous species from post-harvest agricultural-waste burning in source region of the Indo-Gangetic Plain. Tellus B. 66, 21026. https://doi.org/10.3402/tellusb.v66.21026.

Ram, K., Sarin, M., 2009. Absorption coefficient and site-specific mass absorption efficiency of elemental carbon in aerosols over urban, rural, and high-altitude sites in India. Environ. Sci. Technol. 43, 8233–8239.

Ram, K., Sarin, M., 2010. Spatio-temporal variability in atmospheric abundances of EC, OC and WSOC over Northern India. J. Aerosol. Sci. 41 (1), 88–98.

Ram, K., Sarin, M.M., 2015. Atmospheric carbonaceous aerosols from Indo-Gangetic Plain and Central Himalaya: impact of anthropogenic sources. J. Environ. Manag. 148, 153–163.

Ram, K., Sarin, M., Hegde, P., 2010. Long-term record of aerosol optical properties and chemical composition from a high-altitude site (Manora Peak) in Central Himalaya. Atmos. Chem. Phys. 10 (23), 11791–11803.

Ramanathan, V., Carmichael, G.R., 2008. Global and regional climate changes due to black carbon. Nat. Geosci. 1 (4), 221–227.

Ramanathan, V., Li, F., Ramana, M.V., Praveen, P.S., Kim, D., Corrigan, C.E., Nguyen, H., Stone, E.A., Schauer, J.J., Carmichael, G.R., Adhikary, B., Yoon, S.C., 2007. Atmospheric brown clouds: Hemispherical and regional variations in long-range transport, absorption, and radiative forcing. J. Geophys. Res. Atmos. 112, D22S21. https://doi.org/10.1029/2006JD008124.

Ravindra, K., Singh, T., Sinha, V., Sinha, B., Paul, S., Attri, S.D., Mor, S., 2021. Appraisal of regional haze event and its relationship with PM2.5 concentration, crop residue burning and meteorology in Chandigarh, India. Chemosphere 273,. https://doi.org/10.1016/j.chemosphere.2020.128562 128562.

Salam, A., Andersson, A., Jeba, F., Haque, M.I., Khanm, M.D.H., Gustafsson, Ö., 2021. Wintertime air quality in megacity Dhaka, Bangladesh strongly affected by influx of black carbon aerosols from regional biomass burning. Environ. Sci. Technol. 55 (18), 12243–12249.

Saleh, R., Hennigan, C.J., McMeeking, G.R., Chuang, W.K., Robinson, E.S., Coe, H., Donahue, N.M., Robinson, A.L., 2013. Absorptivity of brown carbon in fresh and photo-chemically aged biomass-burning emissions. Atmos. Chem. Phys. 13 (15), 7683–7693.

Sarangi, T., Naja, M., Ohja, N., Kumar, R., Lal, S., Venkataramani, S., Kumar, A., Sagar, R., Chandola, H.C., 2014. First simultaneous measurements of ozone, CO and NOy at a high-altitude regional representative site in the central Himalayas. J. Geophys. Res. Atmos. 119 (3), 1592–1611.

Sharma, S.K., Mandal, T.K., Saxena, M., Sharma, R.A., Datta, A., Saud, T., 2014. Variation of OC, EC, WSIC and trace metals of PM_{10} in Delhi. India. J. Atmos. Sol-Terr. Phy. 113, 10–22.

Sheesley, R.J., Kirillova, E., Andersson, A., Krusa, M., Praveen, P.S., Budhavant, K., Safai, P.D., Rao, P.S.P., Gustafsson, Ö., 2012. Year-round radiocarbon-based source apportionment of carbonaceous aerosols at two background sites in South Asia. J. Geophys. Res. Atmos. 117, D10202. https://doi.org/10.1029/2011JD017161.

Sinha, V., Kumar, V., Sarkar, C., 2014. Chemical composition of pre-monsoon air in the Indo-Gangetic Plain measured using a new air quality facility and PTR-MS: high surface ozone and strong influence of biomass burning. Atmos. Chem. Phys. 14 (12), 5921–5941.

Srinivas, B., Sarin, M.M., 2014. $PM_{2.5}$, EC and OC in atmospheric outflow from the Indo-Gangetic Plain: Temporal variability and aerosol organic carbon-to-organic mass conversion factor. Sci. Total Environ. 487, 196–205.

Sun, H.L., Biedermann, L., Bond, T.C., 2007. Color of brown carbon: A model for ultraviolet and visible light absorption by organic carbon aerosol. Geophys. Res. Lett. 34 (17), L17813. https://doi.org/10.1029/2007GL029797.

Szidat, S., Jenk, T.M., Gaggeler, H., Synal, H., Fisseha, R., Baltensperger, U., Kalberer, M., Samburova, V., Wacker, L., Saurer, M., 2004. Source apportionment of aerosols by ^{14}C measurements in different carbonaceous particle fractions. Radiocarbon. 46, 475–484.

Tripathee, L., Kang, S.C., Rupakheti, D., Cong, Z.Y., Zhang, Q.G., Huang, J., 2017. Chemical characteristics of soluble aerosols over the central Himalayas: insights into spatiotemporal variations and sources. Environ. Sci. Pollut. Res. 24 (31), 24454–24472.

Tripathee, L., Guo, J.M., Kang, S.C., Paudyal, R., Sharma, C.M., Huang, J., Chen, P.F., Ghimire, P.S., Sigdel, M., Sillanpaa, M., 2020. Measurement of mercury, other trace elements and major ions in wet deposition at Jomsom: The semi-arid mountain valley of the Central Himalaya. Atmos. Res. 234,. https://doi.org/10.1016/j.atmosres.2019.104691 104691.

Venkataraman, C., Habib, G., Eiguren-Fernandez, A., Miguel, A.H., Friedlander, S.K., 2005. Residential biofuels in South Asia: Carbonaceous aerosol emissions and climate impacts. Science 307 (5714), 1454–1456.

Verma, S., Ghosh, S., Boucher, O., Wang, R., Menut, L., 2022. Black carbon health impacts in the Indo-Gangetic plain: Exposures, risks, and mitigation. Sci. Adv. 8 (31), eabo4093. https://doi.org/10.1126/sciadv.abo4093.

Wan, X., Kang, S.C., Li, Q.L., Rupakheti, D., Zhang, Q.G., Guo, J.M., Chen, P.F., Tripathee, L., Rupakheti, M., Panday, A.K., Wang, W., Kawamura, K., Gao, S.P., Wu, G.M., Cong, Z.Y., 2017. Organic molecular tracers in the atmospheric aerosols from Lumbini, Nepal, in the northern Indo-Gangetic Plain: influence of biomass burning. Atmos. Chem. Phys. 17 (14), 8867–8885.

Wang, Y.Q., Zhang, X.Y., Draxler, R.R., 2009. TrajStat: GIS-based software that uses various trajectory statistical analysis methods to identify potential sources from long-term air pollution measurement data. Environ. Modell. Softw. 24 (8), 938–939.

Weingartner, E., Saathoff, H., Schnaiter, M., Streit, N., Bitnar, B., Baltensperger, U., 2003. Absorption of light by soot particles: determination of the absorption coefficient by means of Aethalometers. J. Aerosol Sci. 34 (10), 1445–1463.

Winiger, P., Andersson, A., Yttri, K.E., Tunved, P., Gustafsson, Ö., 2015. Isotope-based source apportionment of EC aerosol particles during winter high-pollution events at the Zeppelin Observatory. Svalbard. Environ. Sci. Technol. 49, 11959–11966.

Winiger, P., Andersson, A., Yttri, K.E., Tunved, P., Gustafsson, Ö., 2016. The sources of atmospheric black carbon at a European gateway to the Arctic. Nat. Commun. 7 (1), 12776. https://doi.org/10.1038/ncomms12776.

Winiger, P., Andersson, A., Eckhardt, S., Stohl, A., Semiletov, I.P., Dudarev, O.V., Charkin, A., Shakhova, N., Klimont, Z., Heyes, C., Gustafsson, Ö., 2017. Siberian Arctic black carbon sources constrained by model and observation. Proc. Natl. Acad. Sci. U.S.A. 114 (7), 1054–1061.

Winiger, P., Barrett, T.E., Sheesley, R.J., Huang, L., Sharma, S., Barrie, L.A., Yttri, K.E., Evangeliou, N., Eckhardt, S., Stohl, A., Klimont, Z., Heyes, C., Semiletov, I.P., Dudarev, O.V., Charkin, A., Shakhova, N., Holmstrand, H., Andersson, A., Gustafsson, Ö., 2019. Source apportionment of circum-Arctic atmospheric black caron from isotopes and modeling. Sci. Adv. 5 (2), eaau8052. https://doi.org/10.1126/sciadv.aau8052.

Xu, B.Q., Cao, J.J., Hansenc, J., Yao, T.D., Joswiaa, D.R., Wang, N.L., Wu, G.J., Wang, M., Zhao, H.B., Yang, W., Liu, X.Q., He, J.Q., 2009. Black soot and the survival of Tibetan glaciers. Proc. Natl. Acad. Sci. U.S.A. 106 (52), 22114–22118.

Yang, J.H., Kang, S.C., Ji, Z.M., Chen, D.L., 2018. Modeling the origin of anthropogenic black carbon and its climatic effect over the Tibetan Plateau and surrounding regions. J. Geophys. Res. Atmos. 123 (2), 671–692.

Zencak, Z.M., Elmquist, M., Gustafsson, Q., 2007. Quantification and radiocarbon source apportionment of black carbon in atmospheric aerosols using the CTO-375 method. Atmos. Environ. 41 (36), 7895–7906.

Zhang, Y.L., Li, J., Zhang, G., Zotter, P., Huang, R.J., Tang, J.H., Wacker, L., Prévôt, A.S., Szidat, S.N., 2014. Radiocarbon-based source apportionment of carbonaceous aerosols at a regional background site on Hainan Island. South China. Environ. Sci. Technol. 48 (5), 2651–2659.

Zhang, Y.L., Schnelle-Kreis, J.R., Abbaszade, G.L., Zimmermann, R., Zotter, P., Shen, R. R., Schäfer, K., Shao, L., Prévôt, A.S., Szidat, S.N., 2015. Source apportionment of elemental carbon in Beijing, China: Insights from radiocarbon and organic marker measurements. Environ. Sci. Technol. 49 (14), 8408–8415.

Zhang, Y.L., Kang, S.C., Cong, Z.Y., Schmale, J., Sprenger, M., Li, C.L., Yang, W., Gao, T. G., Sillanpää, M., Li, X.F., Liu, Y.J., Chen, P.F., Zhang, X.L., 2017. Light-absorbing impurities enhance glacier albedo reduction in the southeastern Tibetan Plateau. J. Geophys. Res. Atmos. 122 (13), 6915–6933.